Photon pair generation in a silicon micro-ring resonator with reverse bias enhancement

Erman Engin,[1] Damien Bonneau,[1] Chandra M. Natarajan,[2] Alex S. Clark,[1] M. G. Tanner,[2] R. H. Hadfield,[2] Sanders N. Dorenbos,[3] Val Zwiller,[3] Kazuya Ohira,[4] Nobuo Suzuki,[4] Haruhiko Yoshida,[4] Norio Iizuka,[4] Mizunori Ezaki,[4] Jeremy L. O'Brien,[1] and Mark G. Thompson[1*]

[1]*Centre for Quantum Photonics, H. H. Wills Physics Laboratory & Department of Electrical and Electronic Engineering, University of Bristol, Bristol, UK*
[2]*Scottish Universities Physics Alliance and School of Engineering and Physical Sciences, Heriot-Watt University, Edinburgh, UK*
[3]*Kavli Institute of Nanoscience, TU Delft, The Netherlands*
[4]*Corporate Research & Development Center, Toshiba Corporation, Japan*
[*]*mark.thompson@bristol.ac.uk*

Abstract: Photon sources are fundamental components for any quantum photonic technology. The ability to generate high count-rate and low-noise correlated photon pairs via spontaneous parametric down-conversion using bulk crystals has been the cornerstone of modern quantum optics. However, future practical quantum technologies will require a scalable integration approach, and waveguide-based photon sources with high-count rate and low-noise characteristics will be an essential part of chip-based quantum technologies. Here, we demonstrate photon pair generation through spontaneous four-wave mixing in a silicon micro-ring resonator, reporting separately a maximum coincidence-to-accidental (CAR) ratio of 602 ± 37 (for a generation rate of 827kHz), and a maximum photon pair generation rate of 123 MHz ± 11 kHz (with a CAR value of 37). To overcome free-carrier related performance degradations we have investigated reverse biased p-i-n structures, demonstrating an improvement in the pair generation rate by a factor of up to 2 with negligible impact on CAR.

OCIS codes: (270.0270) Quantum optics; (250.4390) Nonlinear optics, integrated optics.

References and links

1. M. G. Thompson, A. Politi, J. C. F. Matthews, and J. L. O'Brien, "Integrated waveguide circuits for optical quantum computing," Circuits, Devices & Systems, IET **5**(2), 94–102 (2011).
2. A. Politi, M. J. Cryan, J. G. Rarity, S. Yu, and J. L. O'Brien, "Silica-on-silicon waveguide quantum circuits," Science **320**(5876), 646–649 (2008).
3. A. Politi, J. C. F. Matthews, and J. L. O'Brien, "Shor's quantum factoring algorithm on a photonic chip," Science **325**(5945), 1221 (2009).
4. A. Peruzzo, M. Lobino, J. C. F. Matthews, N. Matsuda, A. Politi, K. Poulios, X. Q. Zhou, Y. Lahini, N. Ismail, K. Wörhoff, Y. Bromberg, Y. Silberberg, M. G. Thompson, and J. L. OBrien, "Quantum walks of correlated photons," Science **329**(5998), 1500–1503 (2010).
5. P. J. Shadbolt, M. R. Verde, A. Peruzzo, A. Politi, A. Laing, M. Lobino, J. C. F. Matthews, M. G. Thompson, and J. L. O'Brien, "Generating, manipulating and measuring entanglement and mixture with a reconfigurable photonic circuit," Nat. Photonics **6**(1), 45–49 (2011).
6. J. E. Sharping, K. F. Lee, M. A. Foster, A. C. Turner, B. S. Schmidt, M. Lipson, A. L. Gaeta, and P. Kumar, "Generation of correlated photons in nanoscale silicon waveguides," Opt. Express **14**(25), 12388–12393 (2006).
7. F. Marsili, V. B. Verma, J. A. Stern, S. Harrington, A. E. Lita, T. Gerrits, I. Vayshenker, B. Baek, M. D. Shaw, R. P. Mirin, and S. W. Nam, "Detecting single infrared photons with 93% system efficiency," Nat. Photonics **7**(3), 210–214 (2013).
8. C. Schuck, W. H. P. Pernice, O. Minaeva, M. Li, G. Gol'tsman, A. V. Sergienko, and H. X. Tang, "Matrix of integrated superconducting single-photon detectors with high timing resolution. applied superconductivity," IEEE Transactions on **23**, 2201007–2201014 (2013).
9. D. Bonneau, E. Engin, K. Ohira, N. Suzuki, H. Yoshida, N. Iizuka, M. Ezaki, C. M. Natarajan, M. G. Tanner, R. H. Hadfield, S. N. Dorenbos, V. Zwiller, J. L. O'Brien, and M. G. Thompson, "Quantum interference and

#194423 - $15.00 USD Received 22 Jul 2013; revised 9 Oct 2013; accepted 10 Oct 2013; published 6 Nov 2013

manipulation of entanglement in silicon wire waveguide quantum circuits," New J. Phys. **14**(4), 045003–045014 (2012).
10. X. Xu, Z. Xie, J. Zheng, J. Liang, T. Zhong, M. Yu, S. Kocaman, G. Q. Lo, D. L. Kwong, D. R. Englund, F. N. C. Wong, and C. W. Wong, "Near-infrared Hong-Ou-Mandel interference on a silicon quantum photonic chip," Opt. Express **21**(4), 5014–5024 (2013).
11. C. Xiong, C. Monat, A. S. Clark, C. Grillet, G. D. Marshall, M. J. Steel, J. Li, L. O'Faolain, T. F. Krauss, J. G. Rarity, and B. J. Eggleton, "Slow-light enhanced correlated photon pair generation in a silicon photonic crystal waveguide," Opt. Lett. **36**(17), 3413–3415 (2011).
12. N. Matsuda, H. Takesue, K. Shimizu, Y. Tokura, E. Kuramochi, and M. Notomi, "Slow light enhanced correlated photon pair generation in photonic-crystal coupled-resonator optical waveguides," Opt. Express **21**(7), 8596–8604 (2013).
13. S. Clemmen, K. Phan Huy, W. Bogaerts, R. G. Baets, P. Emplit, and S. Massar, "Continuous wave photon pair generation in silicon-on-insulator waveguides and ring resonators," Opt. Express **17**(19), 16558–16570 (2009).
14. S. Azzini, D. Grassani, M. J. Strain, M. Sorel, L. G. Helt, J. E. Sipe, M. Liscidini, M. Galli, and D. Bajoni, "Ultra-low power generation of twin photons in a compact silicon ring resonator," Opt. Express **20**(21), 23100–23107 (2012).
15. M. G. Tanner, C. M. Natarajan, V. K. Pottapenjara, J. A. O'Connor, R. J. Warburton, R. H. Hadfield, B. Baek, S. Nam, S. N. Dorenbos, B. Urena, T. Zijlstra, T. M. Klapwijk, and V. Zwiller, "Enhanced telecom wavelength single-photon detection with NbTiN superconducting nanowires on oxidized silicon," Appl. Phys. Lett. **96**(22), 221109 (2010).
16. I. D. Rukhlenko, M. Premaratne, and G. P. Agrawal, "Analytical study of optical bistability in silicon ring resonators," Opt. Lett. **35**(1), 55–57 (2010).
17. H. Rong, A. Liu, R. Jones, O. Cohen, D. Hak, R. Nicolaescu, A. Fang, and M. Paniccia, "An all-silicon Raman laser," Nature **433**(7023), 292–294 (2005).
18. A. C. Turner-Foster, M. A. Foster, J. S. Levy, C. B. Poitras, R. Salem, A. L. Gaeta, and M. Lipson, "Ultrashort free-carrier lifetime in low-loss silicon nanowaveguides," Opt. Express **18**(4), 3582–3591 (2010).
19. A. Gajda, L. Zimmermann, J. Bruns, B. Tillack, and K. Petermann, "Design rules for p-i-n diode carriers sweeping in nano-rib waveguides on SOI," Opt. Express **19**(10), 9915–9922 (2011).
20. H. Rong, Y. H. Kuo, A. Liu, M. Paniccia, and O. Cohen, "High efficiency wavelength conversion of 10 Gb/s data in silicon waveguides," Opt. Express **14**(3), 1182–1188 (2006).
21. L. G. Helt, Z. Yang, M. Liscidini, and J. E. Sipe, "Spontaneous four-wave mixing in microring resonators," Opt. Lett. **35**(18), 3006–3008 (2010).
22. A. L. Migdall, D. Branning, and S. Castelletto, "Tailoring single-photon and multiphoton probabilities of a single photon on-demand source," Phys. Rev. A **66**(5), 053805–053809 (2002).
23. K. I. Harada, H. Takesue, H. Fukuda, T. Tsuchizawa, T. Watanabe, K. Yamada, Y. Tokura, and S. I. Itabashi, "Frequency and polarization characteristics of correlated photon-pair generation using a silicon wire waveguide," IEEE J. Sel. Top. Quantum Electron. **16**(1), 325–331 (2010).
24. K. Harada, H. Takesue, H. Fukuda, T. Tsuchizawa, T. Watanabe, K. Yamada, Y. Tokura, and S. Itabashi, "Generation of high-purity entangled photon pairs using silicon wire waveguide," Opt. Express **16**(25), 20368–20373 (2008).

1. Introduction

Integrated quantum photonic circuits are a promising approach to realizing future quantum information processing technologies [1]. Recent demonstrations include quantum logic gates [2], small-scale factoring algorithms [3], quantum simulations [4] and entanglement generation and manipulation [5]. However, these circuits lack the crucial ability to generate quantum-states of light on-chip, and future quantum photonic circuits will require on-chip single-photon sources, single-photon detectors and compact and scalable waveguide circuits to realize applications in quantum communication, sensing, simulations and computation.

The silicon-on-insulator (SOI) material system is a particularly appealing photonic technology platform for realizing future quantum technologies as its high refractive index contrast and mature fabrication techniques provide the ability to implement compact and complex quantum circuits. In addition, the high confinement of light and the large $\chi^{(3)}$ non-linearity of silicon can be utilized for efficient photon-pair generation via spontaneous four-wave mixing (SFWM) [6]. Together with the development of near unity efficient silicon waveguide single-photon detectors [7,8], and the recent demonstration of quantum interference and entanglement manipulation in silicon waveguide circuits [9,10], silicon is a promising platform for fully integrated on-chip quantum photonic technologies.

In this paper we exploit the high $\chi^{(3)}$ nonlinearity of silicon and investigate high Q-factor micro-ring resonators to realize low-noise and high-brightness on-chip photon pair generation. SFWM for photon-pair generation has been previously demonstrated in straight waveguides [6], photonic crystal waveguides [11,12], and micro-ring resonators [13,14]. The

#194423 - $15.00 USD Received 22 Jul 2013; revised 9 Oct 2013; accepted 10 Oct 2013; published 6 Nov 2013

major distinction between these approaches is the generation of broadband photon pairs from the straight waveguides and photonic crystal waveguides, whilst micro-ring resonators can have emission bandwidth orders of magnitude narrower. High Q-factor micro-ring resonators are also able to provide a significant field enhancement, resulting in enhanced photon-pair generation rates. Pair generation enhancement is also observed in photonic crystal waveguides operating in the slow light regime [11,12]. However, due to the large field intensities within these structures, nonlinear optical losses associated with two-photon-absorption (TPA) induced free-carrier-absorption (FCA) can lead to degradation in the performance of the device. Here we present an on-chip photon source with low-noise and high photon-pair count-rate, demonstrating a two-fold performance improvement in count-rate by mitigating these parasitic nonlinear effects. A reverse-biased p-i-n diode is embedded in a silicon micro-ring resonator to remove free-carriers generated by the pump and overcome the FCA associated optical losses. To put this work into context, Table 1 presents a summary of the state-of-the-art in silicon-based photon pair sources focusing on the coincidence-to-accidentals (CAR) performance and associated photon count rates for both pulse excitation and continuous wave excitation.

Table 1. Selection of silicon-based sources in the literature, showing maximum values for CAR and associated photon count rates for pulsed excitation and continuous wave excitation for both straight waveguide sources and ring resonator sources.

Ref	Structure	CAR	Photon pair generation rate
Pulsed Excitation:			
5	9.11mm waveguide	25	2.5MHz
23	1.15cm waveguide	320	0.1MHz
24	1.09cm waveguide	50	0.5MHz
CW Excitation:			
12	1.13cm waveguide	11	9MHz
12	43μm Si ring resonator	30	~0.5MHz
13	20μm Si ring resonator	250	~0.2MHz
this work	73μm Si ring resonator	600	~0.8MHz

2. Experimental setup

Figure 1 shows the experimental setup used. An external-cavity diode laser (ECDL) operating close to 1550 nm provides a pump beam, which is amplified by an erbium-doped fiber amplifier (EDFA) and then spectrally cleaned using a 0.5 nm bandwidth fiber Bragg grating (FBG) and a circulator. This pump beam is then injected into the chip using a 2-μm spot-size lensed fiber. The output containing the residual pump beam and also the photon pairs generated by the SFWM process are collected by another lensed fiber. The pump beam is removed using another FBG-circulator setup and the remaining photon pairs are then separated by a dense-wavelength-division-multiplexer (DWDM) with a 200 GHz channel spacing, and sent to superconducting single photon detectors (SSPD) for time of arrival analysis. We have used SSPDs mounted in a practical closed-cycle refrigerator, with maximum efficiencies of 5% and 15% at 1550 nm [15]. The detection correlation measurement is performed by a time interval analyzer (TIA).

The silicon device is fabricated using an SOI layer structure with a 220 nm silicon layer thickness. The etch depth is 170 nm and the width of the waveguide is 450 nm. The chip is further coated with an oxide layer of thickness 90 nm. The length of the device is 2 mm having spot size converters (300 μm long inverted taper going expanding from 100 nm to 450 nm width) on both the input and the output to efficiently couple the light. The resonator is a racetrack with 10 μm bend radius and 5 μm straight sections and a 300 nm gap between the bus and the racetrack waveguide. We chose the racetrack geometry over a simple ring geometry since it enables to use a larger gap which is more robust to fabrication tolerances. The racetrack waveguide was surrounded by a p-i-n junction formed by ion implantation and

#194423 - $15.00 USD Received 22 Jul 2013; revised 9 Oct 2013; accepted 10 Oct 2013; published 6 Nov 2013

a rapid thermal annealing. The nominal doping concentration was of $1x10^{20}$ cm^{-3} for both p-doping (boron) and n-doping (phosphorous). The distance from each side of the junction to the edge of the waveguide was 400 nm. The coupling losses between the facets and the fiber lenses are estimated to be 3 dB per facet, with a total device insertion loss of ~10 dB. On resonance the device exhibits a 13 dB extinction ratio, and has a Q factor of 37,500. Throughout the experiment we have used TE polarized light.

The resonance wavelength of the micro-ring is controlled via temperature tuning, and when the pump wavelength and the ring resonance are not aligned, we observe photon pair generation from only the 2-mm long straight bus waveguide, as no pump power is coupled to the ring. When the ring and pump are resonant, there is a strong field enhancement in the ring (of length ~70 μm) and an associated increase in the photon-pair generation rate. At high pump powers, TPA of the pump occurs and the resulting free-carrier absorption (FCA), free-carrier dispersion (FCD) and thermo-optical effects give rise to a shift of the ring resonance to a higher wavelength, and an associated reduction in the Q-factor due to the nonlinear losses within the ring. Since we inject a CW pump of a few mW, direct absorption of the pump, signal and idler from TPA is negligible compared to the FCA [16].

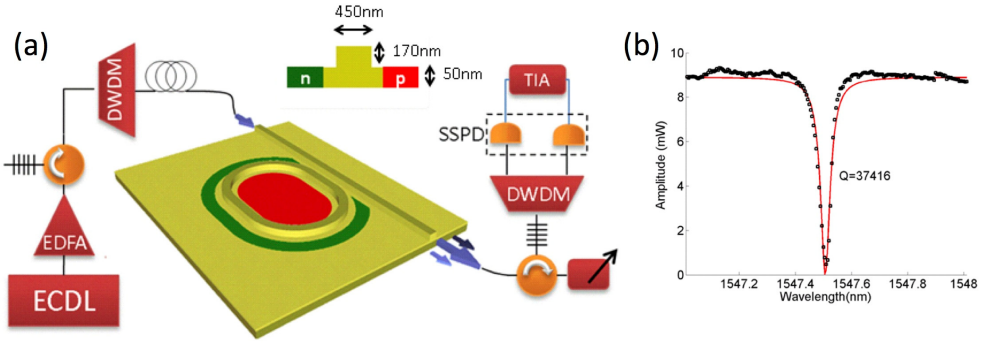

Fig. 1. Experimental setup. A tunable external cavity diode laser (ECDL) is amplified and the noise is removed using a fiber Bragg grating (FBG) with circulator and a dense wavelength division multiplexer (DWDM). The light is coupled in an out of the device using lensed fibers. The output pump and generated photons are separated with another FBG and DWDM. The channels of the DWDM are input into the two channels of the superconducting single photon detector (SSPD) and the response is recorded using a time interval analyzer (TIA). The device is a ring resonator with a 10 μm radius and 5 μm coupling region. The inset shows the cross section of the waveguide and p-i-n junction. b) Transmission spectrum of the device.

3. Results

Figure 2(a) presents the relation between the intrinsic photon pair generation rate and the pump power inside the device. When the ring is off-resonance, the pair generation rate is observed to have a quadratic relationship with the input power, whilst the pair generation rate when the pump is on-resonance are fitted with Eq. (1) derived from the work presented in [16], which accounts for the nonlinear relation between the power inside the ring and the injected pump power.

$$P_{in} = \sqrt{\frac{CC}{\eta_1 \eta_2 \alpha_{ring}}} \frac{1}{t^2} \left(1 - r\tau \left[1 + CC \frac{\beta}{\eta_1 \eta_2 \alpha_{ring}} \right]^{\frac{-1}{4}} \right)^2 \qquad (1)$$

In Eq. (1) *CC* is the number of coincidence counts (pairs) measured per second, α_{ring} is the pair generation coefficient with respect to the power in the ring resonator. *r* and *t* are the reflection and transmission coefficients of the waveguide coupled to the ring, β is the nonlinear coefficient accounting for free carrier absorption, τ is the round trip field

#194423 - $15.00 USD Received 22 Jul 2013; revised 9 Oct 2013; accepted 10 Oct 2013; published 6 Nov 2013

dampening due to losses in the optical waveguide, η_1 and η_2 are the channel collection efficiencies for the signal and idler photons. The power injected to the ring is calculated from the input power accounting for the facet loss.

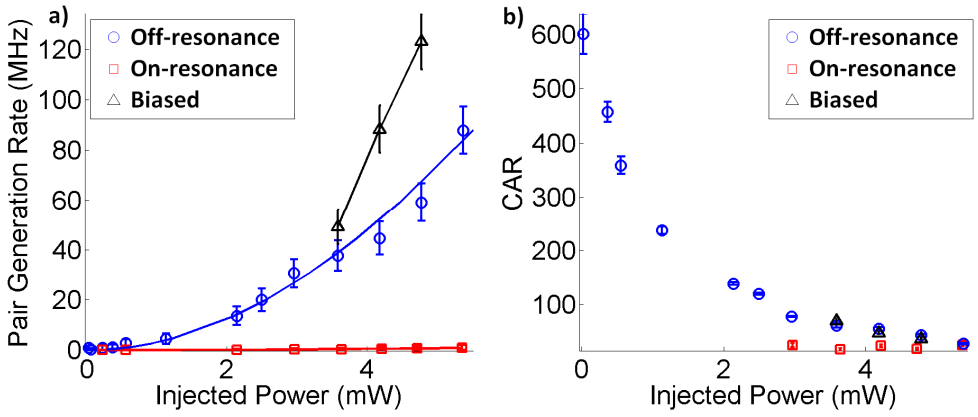

Fig. 2. Results for pair count and CAR. (a) The on-chip photon pair generation rate versus the power input to the device for off-resonance, on-resonance and 8 V reverse bias applied. Count rate is taken as the integral over the FWHM of coincidence histogram. (b) The CAR plotted for these three cases and taken also as the integral over the FWHM - see section 3.2 for more details.

In the off-resonance case, the intrinsic pair generation rate is estimated to be 45 kHz.mW^{-2}, as detailed in section (3.1). In the on-resonance case, we first infer the two channels collection efficiencies η_1 and η_2 (respectively −27 dB and −34 dB) from the measurement of the singles and coincidence counts – see section (3.1). We obtain the ring parameters $t = 0.128$, $r = 0.991$ and $\tau = 0.992$ from the fit to the spectral response of the ring in the linear (low power) regime (Fig. 1(b)). Equation (1) has only then two remaining free parameters and the fit to the curve on Fig. 2(a) gives $\beta = 0.04\text{W}^{-2}$ and $\alpha_{ring} = 0.91$ kHz.mW^{-2}. Then, one can define a low power (i.e. neglecting losses from FCA) pair generation rate (with respect to the input power) as:

$$\alpha = \left(\frac{t}{1-r\tau}\right)^2 \alpha_{ring}$$

giving 3.1MHz.mW^{-2}. For a fixed injected power of 5.3 mW, a comparison of the off- and on-resonance cases gives an enhancement in count rate from 998 kHz to 88 MHz – an 88-fold increase.

It is well known that the large field enhancement of high Q-factor silicon resonators give rise to strong TPA even at relatively low pump powers, generating free-carriers and introducing additional losses which degrade the device performance [17]. In order to mitigate these effects we have incorporated a p-i-n junction surrounding the ring, and by applying a reverse-bias voltage it is possible to sweep out the free carriers generated inside the ring. This approach has previously been shown to reduce the free carrier life-time and suppress free-carrier related effects [18–20], leading for example to an enhanced Raman lasing in silicon [17]. A reverse-bias voltage of 8 V was empirically found to give the best enhancement for the input powers investigated in this work. Figure 2(a) plots the generation rate for the reverse bias case (triangles), showing an enhancement of up to 2.1 times that of the unbiased case (dots) (for an injection power of 4.8 mW), and a maximum count rate of 123 MHz compared with 59 MHz for the un-biased case with the same injection power.

#194423 - $15.00 USD Received 22 Jul 2013; revised 9 Oct 2013; accepted 10 Oct 2013; published 6 Nov 2013

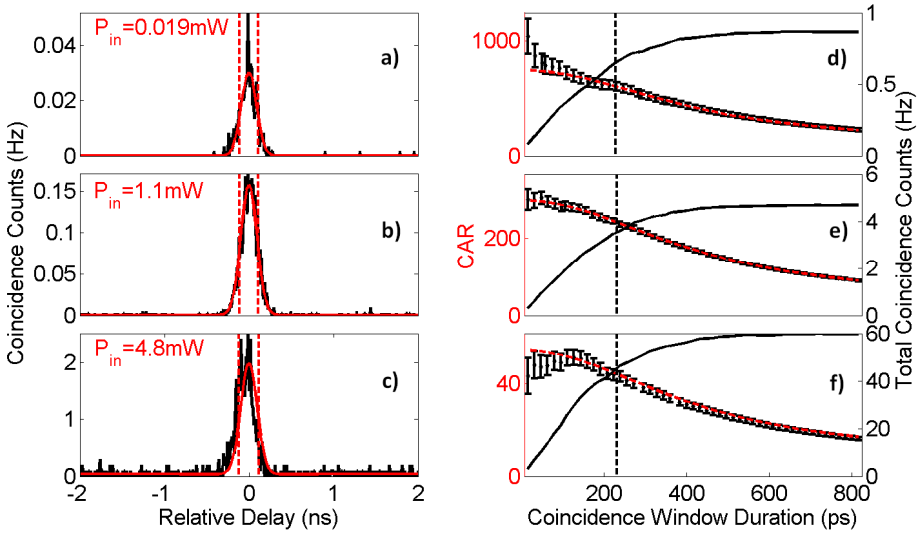

Fig. 3. Extraction of coincidence count-rates and CAR values from the coincidence histogram. (a-c) Coincidence histograms acquired by time interval analysis, with Gaussian fit (red), for different input powers (dotted vertical lines represent the FWHM). (d-f) Total coincident counts (solid, right axis) and CAR values (error bars, left axis) vs. coincidence window duration, calculated from histograms in (a-c). The dashed red curves in (d-f) is the CAR values computed from the Gaussian fit, and the dashed vertical line in (d-f) is the coincidence window durations corresponding to the FWHM of the histograms in (a-c).

The photon-pair generation rates presented in Fig. 2(a) are calculated by acquiring histograms of the coincidence counts for different arrival times of the signal and idler photons (with 8 ps intervals), and then integrating over a coincidence window duration (T) corresponding to the full-width-half-maximum (FWHM) of the coincidence histogram. Figures 3(a)–3(c) present examples of three of these coincidence histograms for three different input powers (0.019, 1.1 and 4.8 mW) for the case of an un-biased on-resonance device. In Figs. 3(d)–3(f), the black solid lines show the total coincidence counts as a function of the coincidence window duration, which tends to a fixed value for coincidence window durations much greater than the FWHM of the coincidence histogram.

3.1 Calculation of pair generation rate

In order to infer the pair generation rates on-chip we have to account for the collection efficiencies of the detection channels which includes all the losses that photons undergo from the chip to the detector and the efficiency of the detector. The collection efficiencies of the two channels and the single and the coincidence counts are related to each other by the following set of formulas.

$$C_1 = \eta_1 \alpha P^2 + \eta_1 P + dc_1 \tag{2}$$

$$C_2 = \eta_2 \alpha P^2 + \eta_2 P + dc_2 \tag{3}$$

$$CC = \eta_1 \eta_2 \alpha P^2 + acc \tag{4}$$

where C_1 and C_2 are the single photon counts, η_1, η_2 are the collection efficiencies of detection channels 1 and 2 respectively, CC is the coincidence count, P is the input power and α is the pair generation rate. The coefficients n_1, n_2 are associated with the noise terms that are linear with respect to the input power (such as Raman noise from the fibers), dc_1 and dc_2 are the dark counts of the two detectors and acc is the accidental counts. The quadratic coefficients of the input power, P in Eqs. (2)–(4) can be extracted from polynomial fits to the measurement data. From these quadratic coefficients it is possible to extract the values for η_1, η_2 and α. We

#194423 - $15.00 USD Received 22 Jul 2013; revised 9 Oct 2013; accepted 10 Oct 2013; published 6 Nov 2013

have integrated the full coincidence histogram peak to obtain the *CC* values in Eq. (4) for low input powers (<2.1mW) in the on-resonance case. The channel collection efficiencies are found to be −27 dB and −34 dB for channel 1 and channel 2 respectively, and take into account all losses within the system (including device coupling losses). These values are used in the calculation of the pair generation rate throughout the experiments.

3.2 Calculation of the CAR

The CAR is calculated by acquiring a histogram of the coincidence counts within an 8 ps detection time interval between signal and idler photons. As already discussed, Figs. 3(a)–3(c) show examples of three coincidence histograms for three different input powers. The CC is defined as the sum of the counts within the given coincidence window. The accidentals are directly measured by integrating the events outside the coincidence peak. By averaging the number of events in each bin outside the coincidence peak and multiplying by the number of bins in one coincidence window, we obtain the number of accidentals. The CAR value and associated CC depends greatly on the duration of the defined coincidence window. Figures 3(d)–3(f) plot this dependence of the CAR and CC on the duration of the chosen coincidence window, calculated using the corresponding histograms in Figs. 3(a)–3(c) respectively. The curves with error-bars in Figs. 3(d)–3(f) show the measured CAR values, and the dashed red curves correspond to CAR values calculated using a Gaussian fit to the histograms in Figs. 3(a)–3(c). As the coincidence window gets wider the values of CAR have a decreasing trend, while the CC saturates at around 2xFWHM. To define a single value of CAR and photon pair generation rate we have used the coincidence window width corresponding to the FWHM of the histograms in Figs. 3(a)–3(c), which is ~230 ps in all cases and is shown as a dotted vertical black line in Figs. 3(d)–3(f).

It can be observed that as the coincidence window duration approaches zero, the CAR values calculated from the Gaussian fit tend to a single value. This value represents that maximum obtainable CAR value from this particular experiment, taking into account all the noise sources including detector dark counts, pump leakage, Raman noise, multi-pair production, etc. It should be noted that the detector dark count rate of 1 kHz, overall collection efficiencies of −27 dB and −34 dB and a coincidence window of 230 ps yield an upper limit on the CAR value of 830. The total coincidence count rate on the other hand tends to a maximum value as the coincidence window duration tends to infinity (and approaches zero as the coincidence window duration tends to zero). Thus to define single values for the photon pair generation rate and CAR, it is necessary to choose a particular coincidence window duration. Typically, the pair generation rates and CAR values quoted in the literature use a range of different and some-what arbitrarily chosen values of the coincidence window. To define the single values for pair generation rate and CAR presented in Fig. 2, we have chosen a coincidence window duration defined as the FWHM of the Gaussian fit to the coincidence peak (the width of the peak is determined by the combined jitter in the single photon detectors, amplifiers and timer interval analyzer and is 230 ps). This enables a useful estimate of the pair generation rate and CAR values by taking into account a significant number of all the coincidence events, yielding values that are close to the maximum obtainable pair generation rates (given as $T \rightarrow$ infinity) and the maximum obtainable CAR (given as $T \rightarrow 0$). It thus provides a useful benchmark for comparison with previous experimental results (see Table 1). Table 2 presents a summary of the photon-pair generation rate and associated CAR for two different coincidence windows; one covering FWHM (~230 ps) and one covering ± 3 standard deviations (~580 ps) of the Gaussian fit to the coincidence histogram.

#194423 - $15.00 USD Received 22 Jul 2013; revised 9 Oct 2013; accepted 10 Oct 2013; published 6 Nov 2013

Table 2. Tabulate results of the CAR and pair generation rate for coincidence window durations covering FWHM and ± 3 standard deviations of the Gaussian fit to the coincidence histogram.

Injection power	CAR (FWHM)	CAR (± 3σ)	Pair generation rate (FWHM)	Pair generation rate (± 3σ)
With 8V reverse bias				
4.8 mW	37 ± 1.3	19 ± 0.6	123 MHz	161 MHz
No reverse bias				
4.8 mW	43 ± 2.2	23 ± 1	59 MHz	75 MHz
1.1 mW	359 ± 16	125 ± 3	2.7 MHz	6 MHz
0.019 mW	602 ± 37	315 ± 18	827 kHz	1 MHz

4. Discussion

In this letter we have studied photon pair generation in a silicon micro-ring resonator through SFWM. A maximum CAR value of 602 ± 37 is measured for an injection pump power of 0.019 mW, corresponding to photon-pair generation rate of 827 kHz. The maximum photon pair generation rate of 123 MHz is achieved, at an injection pump power of 4.8 mW, by applying a 8 V reverse bias voltage across the p-i-n structure to mitigate the parasitic effects of free-carrier absorption (with an associated CAR value of 37 ± 1.3). Increasing the reverse bias voltage beyond 8 V does not lead to a further increase in the photon pair generation rate, and we instead observe a reduction in this rate. We attribute this effect to a change in the coupling constant between the ring resonator and the bus through thermo-optic effects induced by the removal of the free carriers. As we increased the bias voltage, we indeed observed a shift in the resonance peak towards longer wavelengths jointly due to the dominant thermo-optic effect and a reduction in the free carrier dispersion. These free-carrier absorption parasitic effects are even more prominent for devices pumped with short laser pulses. For instance, Xiong et al [11] investigated pair generation in slow-light photonic crystal structures, and demonstrated clear saturation due to TPA and FCA at peak power of just 0.4W. Implementation of a p-i-n structure in such a device could extend the operation of these devices into a regime of higher pair generation rate.

While the photon pair rate increases with reverse bias, it is worth noting that the CAR is only slightly degraded. This degradation is expected from the increase of multi-pair terms due to the higher pair generation rate. However this effect was mitigated by an increase in the signal-idler collection due to the reduced FCA.

The results presented in this paper highlight the potential of silicon as a promising photon source for photonic quantum information processing and communications, with properties of low noise (suitable for example in high fidelity quantum operations) or high generation rate (suitable for example in high-rate quantum key distribution). It is interesting to note from comparing the CAR values shown in Fig. 2(b), we see that for the on-resonance conditions, the reverse-biased and un-biased case give similar values, whereas for off-resonance the CAR is much lower. This is likely due to noise from Raman scattering in optical fibers of the experimental setup which deteriorates the CAR for low photon-pair generation rates in the off-resonance case.

Currently the filtering of the pump, signal and idler photons are achieved using fiber optic components, but with improved architectures, on-chip filtering could also be performed by further taking advantage of resonant structures. The ring cavity also has the advantage of generating photon pairs having low spectral entanglement [21] when pumped with a pulsed source having a bandwidth greater than the resonance width. This will enable such ring sources to be used as high purity single photon sources, heralded on the measurement of one of the photon pairs. The relevant figures of merit (CAR and CC) for such a source should be taken by integrating the full coincidence peak (at least at ± 3σ) since selecting part of the peak would be equivalent to a loss on the heralded photon generated thus lowering the heralding efficiency of the source. The high CAR achieved makes these sources a good candidate for

#194423 - $15.00 USD Received 22 Jul 2013; revised 9 Oct 2013; accepted 10 Oct 2013; published 6 Nov 2013

low noise multiplexed single photon sources [22] which could in turn be used in a scalable manner to seed a linear optical quantum circuit.

The on-chip photon pair source reported in this paper is fully compatible with already demonstrated silicon quantum circuits [9] and high-efficiency waveguide integrated superconducting single-photon detectors [7,8]. It is therefore possible to realize in a single material system all the major components required for on-chip linear optics quantum information processing; low noise single photon sources, compact waveguide circuits and efficient single photon detectors. The next major challenge is to integrate all these components into a single unified technology platform, for which the silicon-on-insulator material system appears to be a promising candidate.

Acknowledgments

We acknowledge John Rarity, Graham Marshall and Joshua Silverstone for useful discussions. This work was supported by EPSRC, ERC, the Centre for Nanoscience and Quantum Information (NSQI) and the European FP7 project QUANTIP. MGT acknowledges support from the Toshiba Research Fellowship scheme. JLO'B acknowledges a Royal Society Wolfson Merit Award. RHH acknowledges a Royal Society University Research Fellowship.

#194423 - $15.00 USD Received 22 Jul 2013; revised 9 Oct 2013; accepted 10 Oct 2013; published 6 Nov 2013